Supporting Information

Construction of three-dimensional Cobalt Sulfide /Multi-Heteroatoms Co-doped Porous Carbon as Efficient Trifunctional Electrocatalyst

*Jiakun Zhang, Bolan Cui, Shang Jiang, Haitao Liu, Meiling Dou**

State Key Laboratory of Chemical Resource Engineering, Laboratory of Electrochemical Process and Technology for materials, Beijing University of Chemical Technology, Beijing 100029, China

Corresponding author: Prof. Meiling Dou, E-mail: douml@mail.buct.edu.cn

1. Experimental Section

1.1. Materials Characterizations

Scanning electron microscopy (SEM) and high-resolution transmission electron microscopy (HR-TEM) characterizations were performed on FE-JSM-6701F (JEOL, Japan) and JSM-2100 (JEOL, Japan) microscopes, respectively. Power X-ray diffraction (XRD) patterns were profiled on an X-ray diffractometer (D/max-2500, Rigaku, Japan) (Cu K_α radiation (λ=1.54056 Å) as the X-ray source). Thermogravimetry (TG) measurements were conducted with a STA 7300 instrument to analyze the sulfidation process under high temperature. The specific surface area and pore size distribution were investigated by nitrogen adsorption-desorption measurements on a Quantachrome AUTOSORB-SI instrument. Raman spectra were obtained on a Horiba Jobin Yvon LabRam HR800 confocal microscope using 632.8 nm as laser. X-ray photoelectron spectroscopy (XPS) measurements were performed on the ESCALAB 250 spectrometer (Thermo Fisher) (using C 1*s* peak (284.98 eV) as reference for calibration).

1.2. Electrochemical Performance Test

For the electrochemical test, a conventional three-electrode system was employed on a CHI760e workstation (Shanghai Chenhua Instrument Corporation, China) using a graphite rod and a saturated calomel electrode (SCE) as the counter and reference electrode, respectively. The electrocatalyst coated rotating ring-disk electrode (RRDE) (area=0.19625 cm^2, from Pine Instrument Company) was used as the working electrode. Typically, 5 mg of the as-prepared electrocatalyst was first added into 1 mL

of isopropanol and then mixed with 10 μL of Nafion (5 wt.%, DuPont) solution by ultrasonically dispersing for 0.5 h. Afterwards, 20 μL of the homogeneous slurry was uniformly dropped on to the RRDE with catalyst loading of 788 μg cm^{-2}. For OER and HER measurements, 10 μL of the above electrocatalyst ink was coated onto glassy carbon electrode (GCE) and dried naturally with the electrocatalyst loading of 394 μg cm^{-2}. For comparison, the commercial Pt/C (20 wt.% of Pt, Johnson Matthey (JM)) and RuO_2 working electrodes were also prepared by ultrasonically dispersing Pt/C or RuO_2 into isopropanol solution containing Nafion (Pt loading: 78.8 and 394 μg cm^{-2} for ORR and HER, respectively; RuO_2 loading: 394 μg cm^{-2}). All potentials are given in reference to the reversible hydrogen electrode (RHE).

1.3. Rechargeable Zn-air Assembly and Performance Test

The rechargeable Zn–air battery was assembled by using a Zn plate and a catalyst-loaded air electrode as the anode and cathode, respectively. 6.0 mol L^{-1} of KOH containing 0.2 mol L^{-1} of $Zn(Ac)_2$ was used as the electrolyte. For the preparation of working electrode, 2.25 mg of the as-prepared electrocatalyst was first added into 1 mL of isopropanol and then mixed with 10 μL of Nafion (5 wt.%, DuPont) solution by ultrasonically dispersing for 0.5 h. For comparison, the commercial Pt/C and IrO_2 electrodes were also prepared by ultrasonically dispersing Pt/C or IrO_2 electrocatalysts into isopropanol solution containing Nafion. All of the homogeneous slurry was dropped on to the carbon fiber with electrocatalyst loading of 1 mg cm^{-2}. The effective area was controlled to be 1 cm^2 for both cathode and anode. All the electrochemical tests of Zn–air battery were conducted on the CHI760e electrochemical workstation.

The durability of the batteries was evaluated by galvanostatic discharge-charge cycling tests (600 s discharging, followed by 600 s charging in each cycle) at a current density of 10 mA cm^{-2}.

1.4. Overall Water Splitting Assembly and Performance Test

The overall water splitting performance was measured in a typical two-electrode system by the CHI 760e electrochemical workstation using the as-prepared electrocatalysts as both cathode and anode. 1 mg of the as-prepared electrocatalyst was first added into 1 mL of isopropanol and then mixed with 10 μL of Nafion (5 wt.%, DuPont) solution by ultrasonically dispersing for 0.5 h. 1 mol L^{-1} of KOH was used as the electrolyte. Cathode and anode were prepared by dispersing the catalysts ink onto carbon cloth (CC) with a loading of 1.0 mg cm^{-2} and dried overnight. Polarization curves were tested in 1 M KOH with a scan rate of 5 mV s^{-1} and the durability of the catalysts was also evaluated via chronopotentiometry test at a current density of 10 mA cm^{-2} for 55000 s.

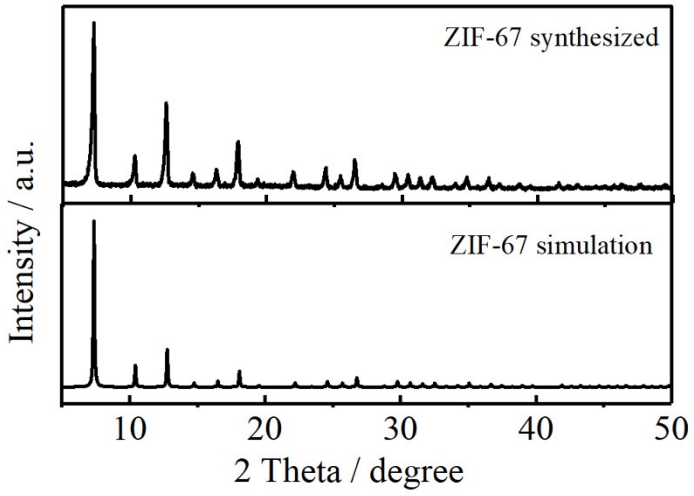

Fig. S1. XRD patterns of ZIF-67.

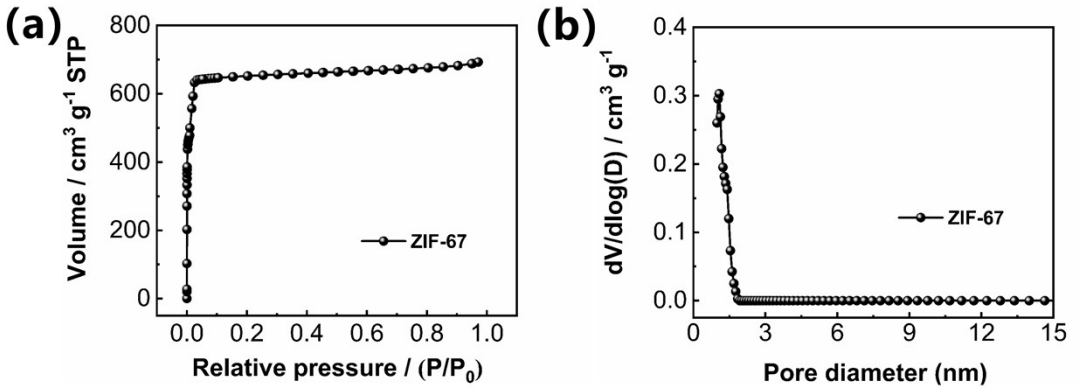

Fig. S2. (a) Nitrogen sorption isotherms and (b) pore size distribution of ZIF-67.

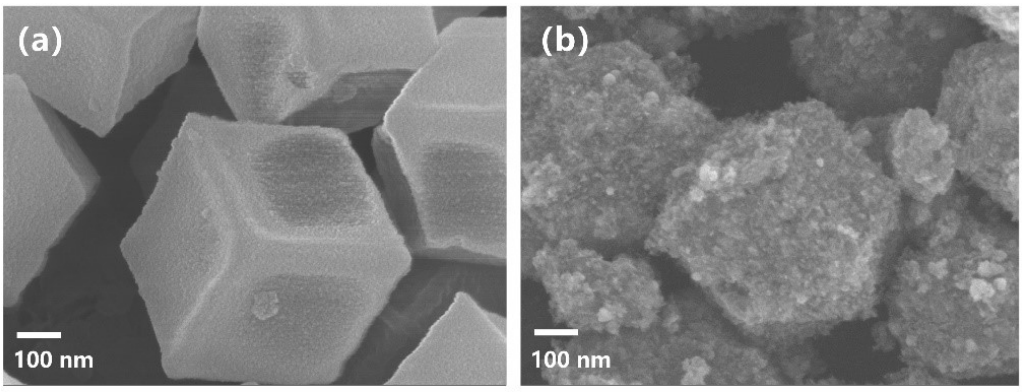

Fig. S3. Representative SEM images (a) of ZIF-67 and (b) Co_9S_8/CoNSC.

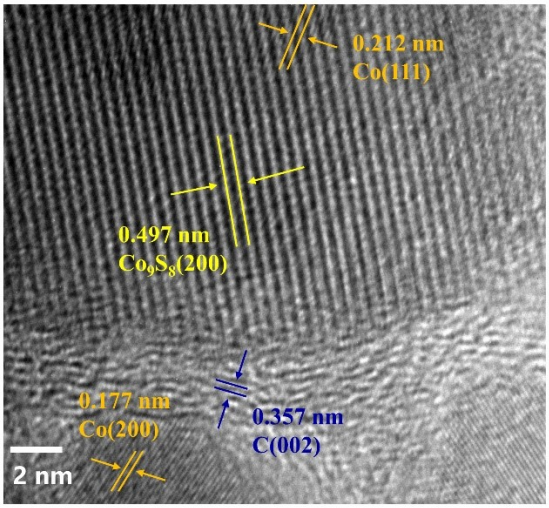

Fig. S4. HR-TEM images of Co_9S_8/CoNSC.

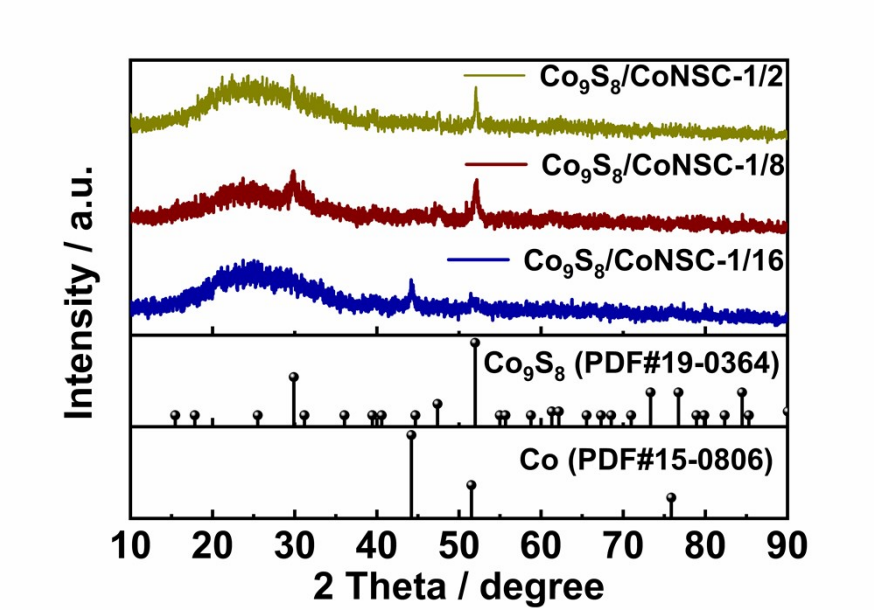

Fig. S5. XRD patterns of Co_9S_8/CoNSC prepared at different mass ratio of S/ZIF-67 (1/2, 1/8 and 1/16).

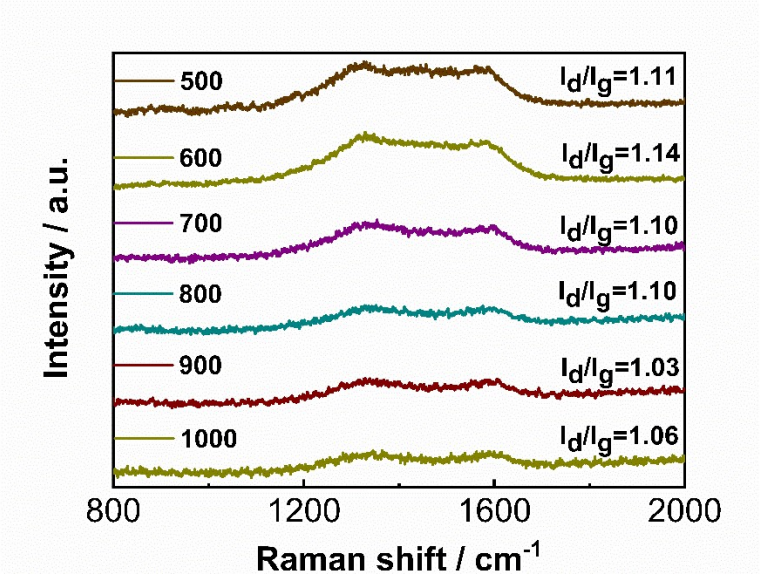

Fig. S6. Raman spectra of Co_9S_8/CoNSC prepared with different temperature.

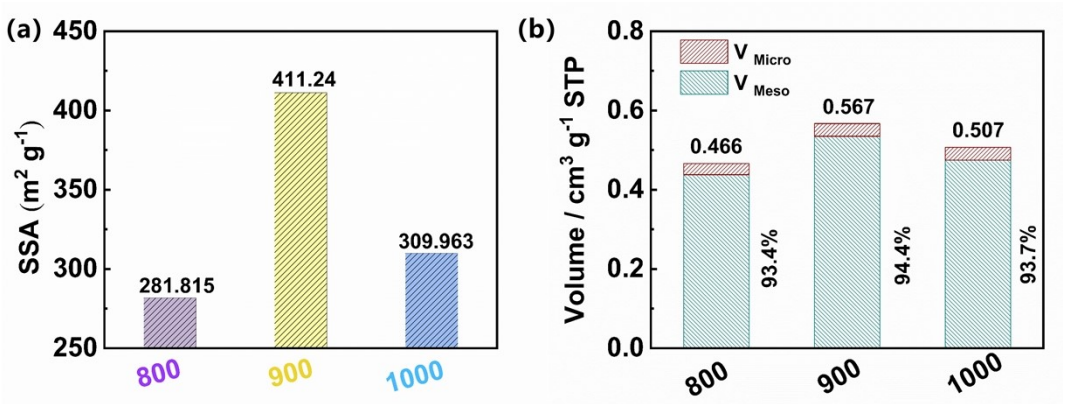

Fig. S7. Summary of (a) specific surface area and (b) pore volume of Co_9S_8/CoNSC.

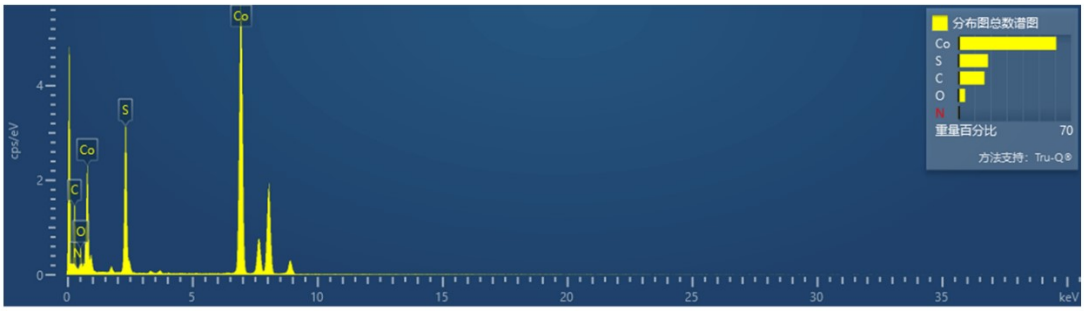

Fig. S8. EDX analysis of Co_9S_8/CoNSC.

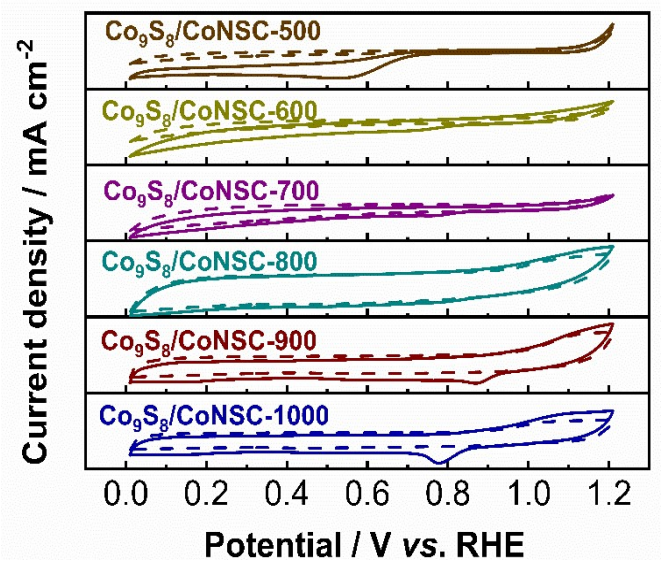

Fig. S9. CV curves of Co_9S_8/CoNSC in N_2- and O_2-saturated 0.1 M KOH.

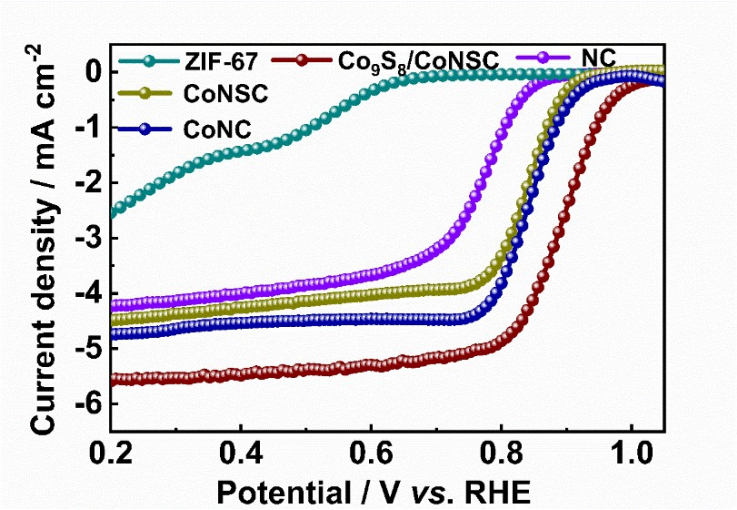

Fig. S10. LSV curves of ZIF-67, CoNSC, CoNC, NC and Co_9S_8/CoNSC in 0.1 M KOH at a scan rate of 5 mV s^{-1}.

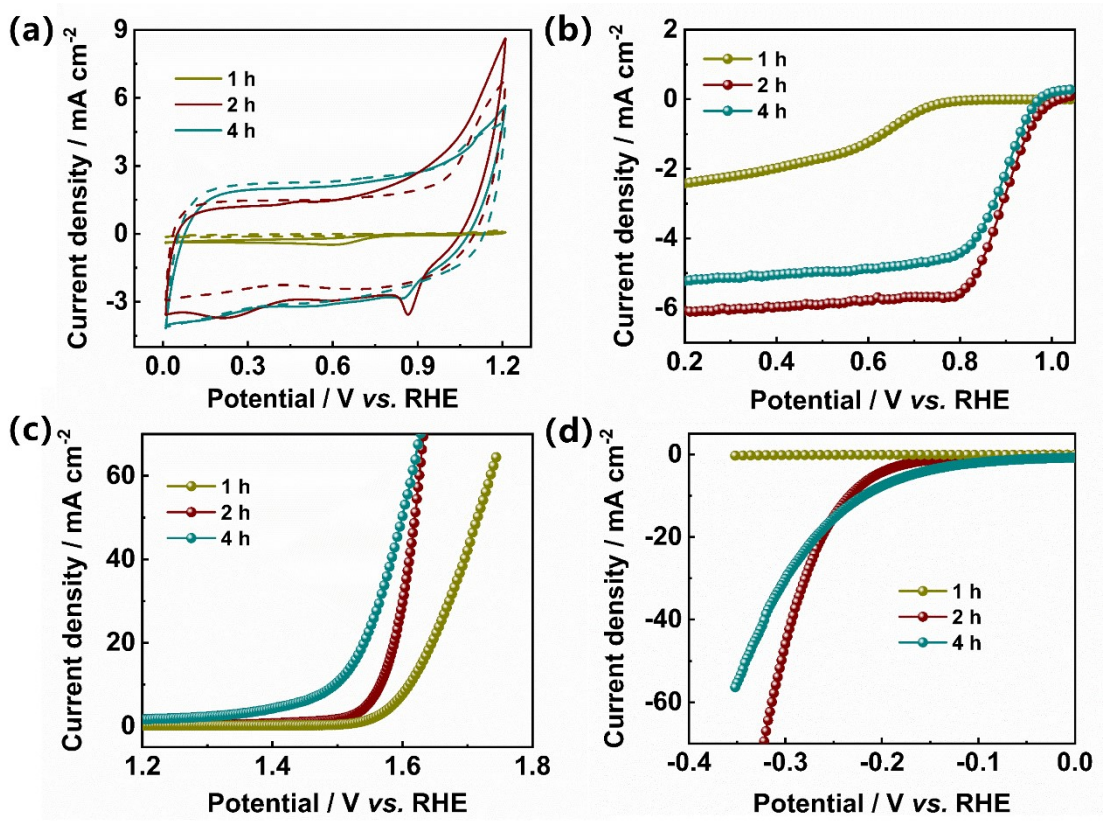

Fig. S11. (a) CV curves of the samples prepared at the sulfidation holding time of 1, 2 and 4 h (at 900 °C) in N_2 (dotted line) and O_2-saturated (solid line) 0.1 M KOH. LSV curves of the samples prepared at holding time of 1, 2 and 4 h (b) toward ORR in 0.1 M KOH at a scan rate of 5 mV s^{-1} in the range 0-1.2 V *vs.* RHE, (c) toward OER in 1 M KOH at a scan rate of 10 mV s^{-1} in the range (0.947)-1.747 V *vs.* RHE and (d) toward

HER in the range (-0.353)-0.147 V *vs.* RHE.

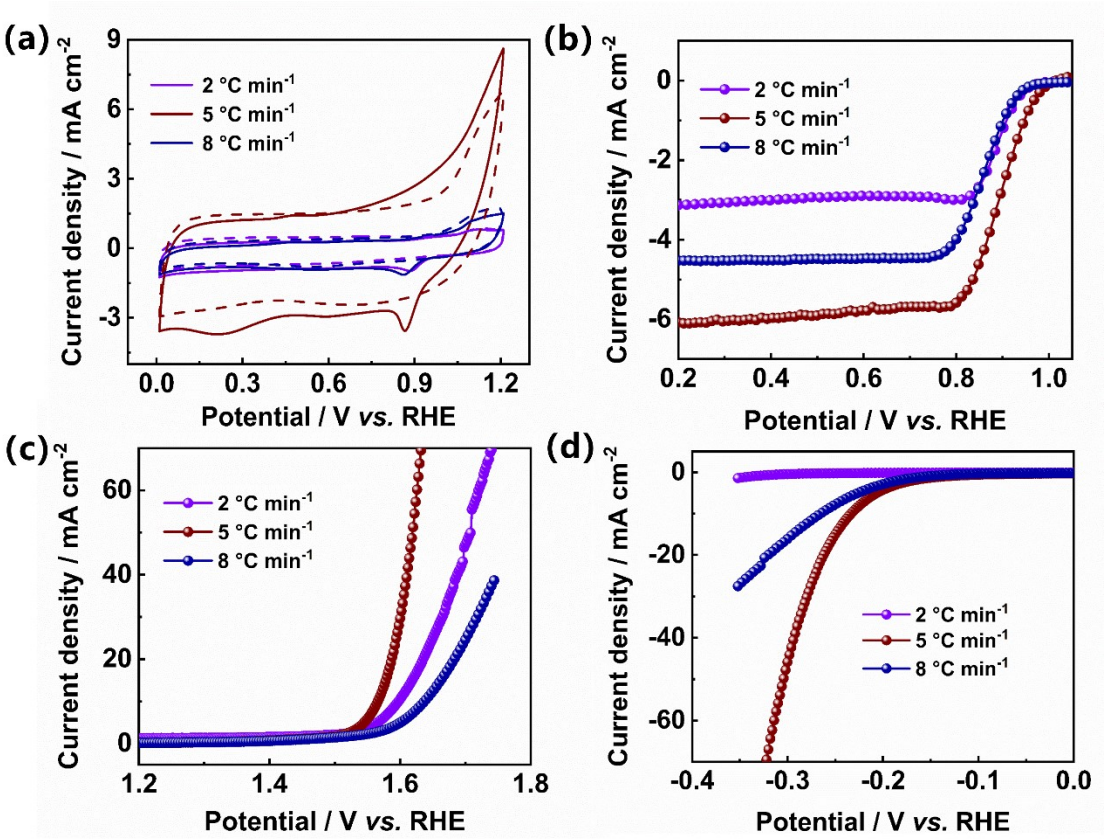

Fig. S12. (a) CV curves of the samples prepared at the sulfidation heating rate of 2, 5 and 8 °C min^{-1} (at 900 °C) in N_2 (dotted line) and O_2-saturated (solid line) 0.1 M KOH. LSV curves of the samples prepared at heating rate of 2, 5 and 8 °C min^{-1} (b) toward ORR in 0.1 M KOH at a scan rate of 5 mV s^{-1} in the range 0-1.2 V *vs.* RHE, (c) toward OER in 1 M KOH at a scan rate of 10 mV s^{-1} in the range (0.947)-1.747 V *vs.* RHE and (d) toward HER in the range (-0.353)-0.147 V *vs.* RHE.

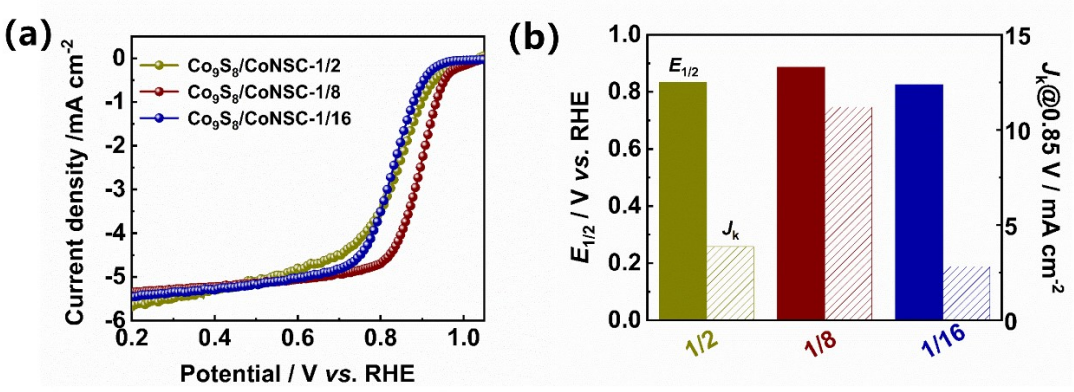

Fig. S13. (a) LSV curves of Co_9S_8/CoNSC prepared at different mass ratio of S/ZIF-67

(1/2, 1/8 and 1/16) in 0.1 M KOH at a scan rate of 5 mV s^{-1} and (b) summary of $E_{1/2}$ and J_k for the above electrocatalysts.

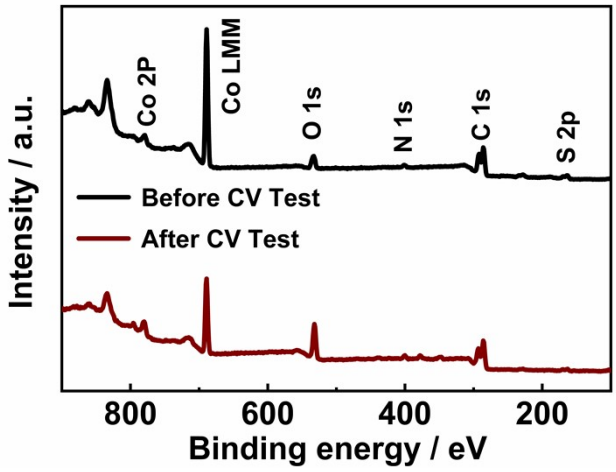

Fig. S14. XPS survey spectra of Co_9S_8/CoNSC before / after CV test toward ORR.

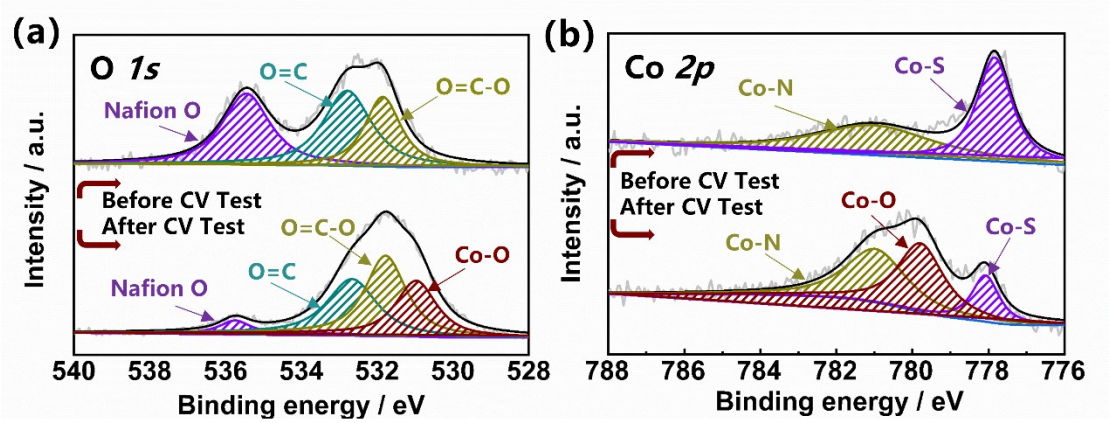

Fig. S15. (a) High-resolution XPS spectra of O 1s and (b) Co 2p of Co9S8/CoNSC before and after CV test toward ORR.

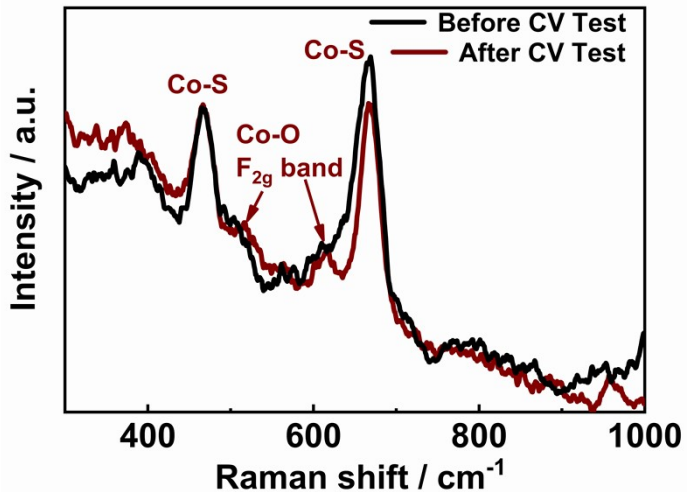

Fig. S16. Raman spectra of Co_9S_8/CoNSC before and after CV test towards ORR.

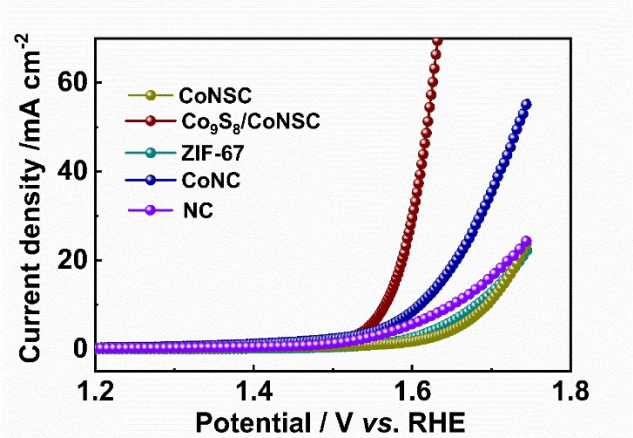

Fig. S17. LSV curves of ZIF-67, CoNSC, CoNC and Co_9S_8/CoNSC in 1 M KOH at a scan rate of 10 mV s^{-1}.

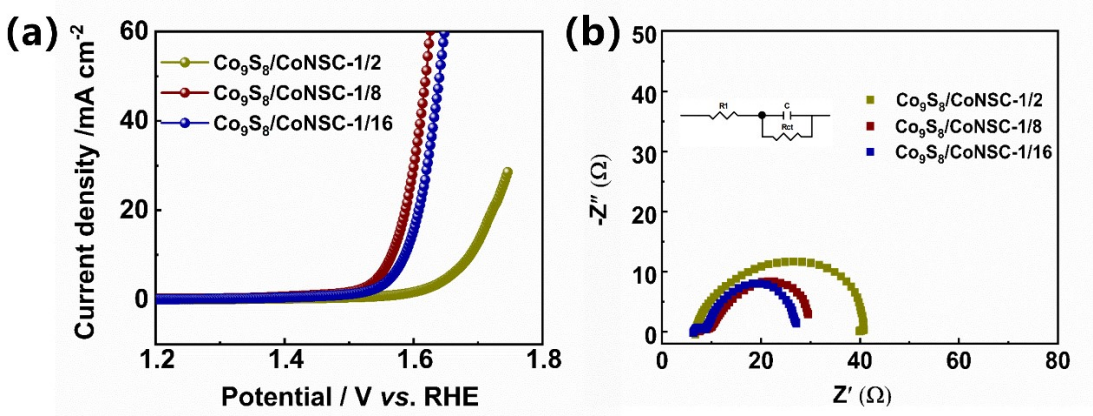

Fig. S18. (a) LSV curves of Co_9S_8/CoNSC prepared at different mass ratio of S/ZIF-67 (1/2, 1/8 and 1/16) in 1 M KOH at a scan rate of 10 mV s^{-1} and (b) Nyquist plots o for the above electrocatalysts.

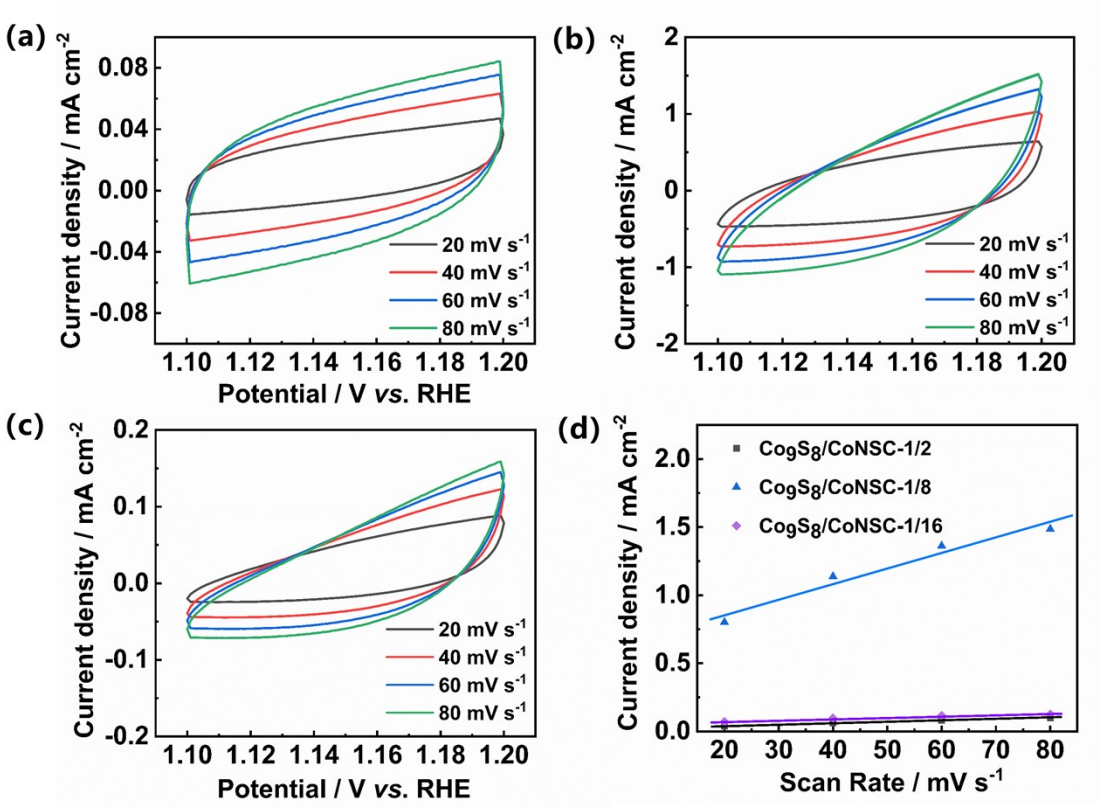

Fig. S19. CV curves of (a) Co_9S_8/CoNSC-1/2, (b) Co_9S_8/CNSC-1/8, (c)Co_9S_8/CNSC-1/16 in 1 M KOH electrolyte for OER during the potential range of 1.1-1.2 V *vs*. RHE and (d) relation of current density versus scan rate for Co_9S_8/CoNSC prepared at different mass ratio of ZIF-67/S.

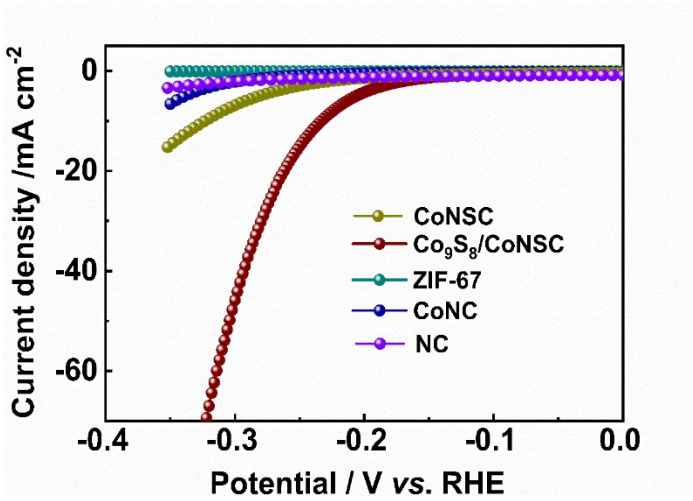

Fig. S20. LSV curves of ZIF-67, CoNSC, CoNC and Co_9S_8/CoNSC in 1 M KOH at a scan rate of 10 mV s^{-1}.

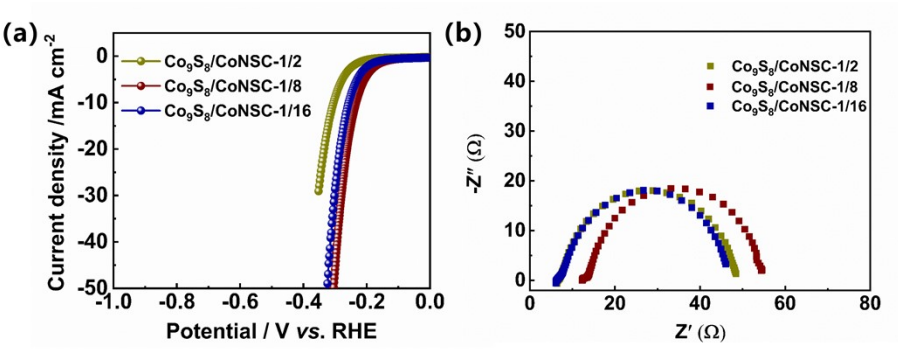

Fig. S21. (a) LSV curves of Co_9S_8/CoNSC prepared at different mass ratio of ZIF-67/S (2, 8 and 16) in 1 M KOH at a scan rate of 10 mV s^{-1} and (b) Nyquist plots o for the above electrocatalysts.

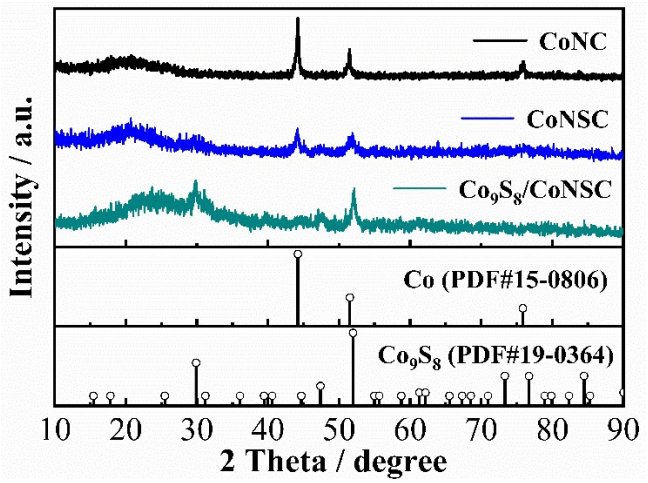

Fig. S22. XRD patterns of CoNC, CoNSC and Co_9S_8/CoNSC

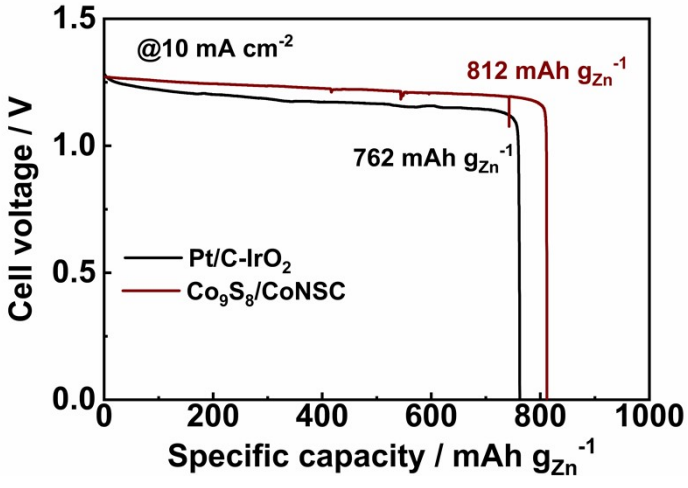

Fig. S23. Discharge curves of Zn–air batteries based on the Co_9S_8/CoNSC and Pt/C-IrO_2 electrodes at 10 mA cm^{-2}.

Table S1. Element composition and content for Co_9S_8/CoNSC based on XPS analysis.

Sample	Co (%)	S (%)	N (%)	C (%)	O (%)
Co_9S_8/CoNSC-500	8.56	11.49	15.38	48.32	16.26
Co_9S_8/CoNSC-600	8.76	9.66	13.8	51.57	16.2
Co_9S_8/CoNSC-700	9.23	12.12	9.24	48.76	20.65
Co_9S_8/CoNSC-800	9.07	13.05	6.71	61.58	9.6
Co_9S_8/CoNSC-900	10.43	15.37	4.84	62.4	6.96
Co_9S_8/CoNSC-1000	7.78	12.03	3.35	70.71	6.13

Table S2. Summary of ORR performance of Co_xS-based materials in 0.1 M KOH.

Materials	E_{onset} (V *vs.* RHE)	$E_{1/2}$ (V *vs.* RHE)	Loading (mg cm^{-2})	Reference
Co_9S_8@NSCM	0.97	0.81	0.15	[1]
Co_9S_8@NC	0.92	0.861	0.248	[2]
Co_9S_8/CD@NSC	/	0.84	0.255	[3]
Ni_3Fe−Co_9S_8/rGO	0.91	0.80	0.25	[4]
CoS_2/Cu_2S-NF	/	0.80	0.265	[5]
Co_9S_8/CoNSC	**0.983**	**0.889**	**0.788**	**This work**

Table S3. XPS results for the Co_9S_8/CoNSC sample before and after CV test.

Element	Co (at. %)	S (at. %)	N (at. %)	C (at. %)	O (at. %)
Before test	1.89	6.19	4.35	77.24	10.33
After test	2.11	2.76	3.65	70.42	21.06

Table S4. Summary of previously reported non-precious metal electrocatalysts for OER in 1.0 M KOH.

Materials	Overpotential @ J_{10}/mV	Loading (mg cm^{-2})	Reference
Co_9S_8@MoS_2	340	0.40	[6]
Co_9S_8@TDC	330	1.4	[7]
Co_9S_8/NSCP	370	0.331	[8]
CeO_x/CoS	269	0.2	[9]
Co_xS_y@C	470	0.141	[10]
Co_9S_8@SNC	320	0.22	[11]
Co_9S_8@NOSC	340	0.28	[12]
Ni_3S_2 nanosheet	260	4.1	[13]
Ni_2P	290	0.25	[14]
CoMnP	330	0.285	[15]
NiCo-LDH	335	1	[16]
Co_4N	330	0.83	[17]
Co_9S_8/CoNSC-900-4 h	**266**	**0.394**	**This work**
Co_9S_8/CoNSC-900-2 h	**326**	**0.394**	**This work**
Co_9S_8/CoNSC-900-1 h	**368**	**0.394**	**This work**
Co_9S_8/CoNSC-900-2 °C min^{-1}	**370**	**0.394**	**This work**
Co_9S_8/CoNSC-900-8 °C min^{-1}	**407**	**0.394**	**This work**

Table S5. Summary of TMCs-based electrocatalysts for HER in 1.0 M KOH.

Materials	Overpotential @ j_{10} / mV	Tafel slope (mV dec^{-1})	Reference
MoS_2@CoS_2	96	60	[18]
Co_9S_8-NDCL	146	70	[19]
Co_9S_8 HNSs	267	139	[20]
Co_9S_8 nanotubes	280	135	[21]
Co_9S_8-Ni_3S_2/NF	277	171	[22]
Co_9S_8/CoNSC	**233**	**93.78**	**This work**

Table S6. Summary of performance for Zn-air battery.

Materials	Power density (mW cm^{-2})	Specific Capacity (mA h g_{Zn}^{-1})	Energy density (Wh kg_{Zn}^{-1})	Cycling stability (h)	Reference
NPS-G	151	686	805	20	[23]
CoO/N-CNT	265	570	700	22	[24]
$Co_{1-x}S/Co_9S_8$	168.2	817.9	973.3	78	[25]
Co/NGC-3	134.4	716	847.4	120	[26]
Co/Co_9S_8-NCL	112	799	/	25	[27]
Co_9S_8/CoNSC	**150**	**812**	**939.5**	**40**	**This work**

Table S7. Summary of performance for overall water splitting in 1.0 M KOH.

Materials	Overpotential @ 10 mA cm^{-2}	Cycling Stability (h)	Reference
Co_9S_8−NSC@Mo_2C	1.61 V	20	[28]
Co_9S_8@MoS_2	1.67 V	16	[29]
Co_9S_8-V_3S_4	1.53 V	48	[30]
MoS_2/NiS_2	1.63V	24	[31]
Co_9S_8@$NiCo_2O_4$	1.55 V	50	[32]

Co_9S_8/CoNSC	**1.585 V**	**34**	**This work**

REFERENCES

1 Y. Li, W. Zhou, J. Dong, Y. Luo, P. An, J. Liu, X. Wu, G. Xu, H. Zhang and J. Zhang, *Nanoscale*, 2018, **10**, 2649-2657.

2 F. Bai, X. Qu, J. Wang, X. Chen and W. Yang, *ACS Appl. Mater. Interfaces*, 2020, **12**, 33740-33750.

3 P. Zhang, D. Bin, J. S. Wei, X. Q. Niu, X. B. Chen, Y. Y. Xia and H. M. Xiong, *ACS Appl. Mater. Interfaces*, 2019, **11**, 14085-14094.

4 X. Hu, T. Huang, Y. Tang, G. Fu and J. M. Lee, *ACS Appl. Mater. Interfaces*, 20 19, **11**, 4028-4036.

5 Y. Z. Chen, C. Wang, Z. Y. Wu, Y. Xiong, Q. Xu, S. H. Yu and H. L. Jiang, *Adv. Funct. Mater.*, 2015, **27**, 5010-5016.

6 J. Li, G. Li, J. Wang, C. Xue, X. Li, S. Wang, B. Han, M. Yang and L. Li, *Inorg. Chem. Front.*, 2020, **7**, 191-197.

7 J.-Y. Zhao, R. Wang, S. Wang, Y.-R. Lv, H. Xu and S.-Q. Zang, *J. Mater. Chem. A*, 2019, **7**, 7389-7395.

8 X. Gao, Z. Xu and G. Li, *Chem. Eng. J.*, 2022, **431**, 133385.

9 N. Huang, S. Yan, L. Yang, M. Zhang, P. Sun, X. Lv and X. Sun, *J. Solid State Chem.*, 2020, **285**, 121185.

10 B. Chen, R. Li, G. Ma, X. Gou, Y. Zhu and Y. Xia, *Nanoscale*, 2015, **7**, 20674-20684.

11 F. Xu, J. Zhao, J. Wang, T. Guan and K. Li, *J. Colloid Interface Sci.*, 2022, **608**, 2623-2632.

12 S. Huang, Y. Meng, S. He, A. Goswami, Q. Wu, J. Li, S. Tong, T. Asefa and M. Wu, *Adv. Funct. Mater.*, 2017, **27**, 1606585.

13 X. Xu, F. Song and X. Hu, *Nat. Commun.*, 2016, **7**, 12324.

14 M. Liu and J. Li, *ACS Appl. Mater. Interfaces*, 2016, **8**, 2158–2165.

15 P. Chen, K. Xu, Z. Fang, Y. Tong, J. Wu, X. Lu, X. Peng, H. Ding, C. Wu and Y. Xie, *Angew. Chem., Int. Ed.*, 2015, **54**, 14710–14714.

16 J. S. Chen, J. Ren, M. Shalom, T. Fellinger and M. Antonietti, *ACS Appl. Mater. Interfaces*, 2016, **8**, 5509–5516.

17 T. Liu , Y. Liang , Q. Liu , X. Sun , Y. He and A. M. Asiri , *Electrochem. Commun.*, 2015, **60** , 92 —96.

18 S. He, H. Du, K. Wang, Q. Liu, J. Sun, Y. Liu, Z. Du, L. Xie, W. Ai and W. Huang, *Chem. Commun* , 2020, **56**, 5548-5551.

19 J. Mujtaba, L. He, H. Zhu, Z. Xiao, G. Huang, A. A. Solovev and Y. Mei, *ACS Appl. Nano Mater.*, 2021, **4**, 1776-1785.

20 X. Ma, W. Zhang, Y. Deng, C. Zhong, W. Hu and X. Han, *Nanoscale*, 2018, **10**, 4816-4824.

21 L. Jin, C. Lv, J. Wang, H. Xia, Y. Zhao and Z. Huang, *J. Anal. Chem.*, 2016, **7**, 210-218.

22 R. Illathvalappil, P. S. Walko, F. Kanheerampockil, S. K. Bhat, R. N. Devi and S. Kurungot, *Chem. Eur. J.*, 2020, **26**, 7900-7911.

23 X. Zheng, J. Wu, X. Cao, J. Abbott, C. Jin, H. Wang, P. Strasser, R. Yang, X. Chen and G. Wu, *Appl. Catal. B-Environ.*, 2019, **241**, 442-451.
24 Y. G. Li, M. Gong, Y. Liang, J. Feng, J. E. Kim, H. Wang and H. J. Dai, *Nat. Commun.*, 2013, **4**, 1805.
25 B. N. Wang, D. Chen, H. Z. Dong, Y. Huang, L. Sui, B. L. Pang and L. F. Dong, *Electrochim. Acta*, 2021, **388**, 138594.
26 J. M. Li, Y. M. Kang, D. Liu, Z. Q. Lei and P. Liu. *ACS Appl. Mater. Interfaces*, 2020, **12**, 5717-5729.
27 N.-F. Yu, C. Wu, W. Huang, Y.-H. Chen, D.-Q. Ruan, K.-L. Bao, H. Chen, Y. Zhang, Y. Zhu, Q.-H. Huang, W.-H. Lai, Y.-X. Wang, H.-G. Liao, S.-G. Sun, Y.-P. Wu and J. Wang, *Nano Energy*, 2020, **77**.
28 X. H. Luo, Q. L. Zhou, S. Du, J. W. Zhong, X. L. Deng and Y. L. Liu, *ACS Appl. Mater. Interfaces*, 2018, **10**, 22291-22302.
29 J. M. Bai, T. Meng, D. L. Guo, S. G. Wang, B. G. Mao and M. H. Cao, *ACS Appl. Mater. Interfaces*, 2018, **2**, 1678-1689.
30 X. Dong, Y. Q. Jiao, G. C. Yang, H. J. Yan, A. Wu, D. Z. Guo, Y. Wang, C. G. Tian and H. G. Fu, *Sci China Mater*, 2021, **64**, 1396-1407.
31 J. Xu, J. Rong, Y. Zheng, Y. Zhu, K. Mao, Z. Jing, T. Zhang, D. Yang and F. Qiu, *Electrochim. Acta*, 2021, **385**, 138438.
32 X. Q. Du, C. Y. Zhang, H. B. Wang, Y. H. Wang and X. S. Zhang. *J. Alloys Compd.*, 2021, **885**, 160972.